

Mass parameter in nuclear quadrupole motion*

P. K. Haff

*University of Washington, Seattle, Washington 98105,
and California Institute of Technology, Pasadena, California 91109*

L. Wilets

University of Washington, Seattle, Washington 98105

(Received 22 January 1974)

The self-cranked generator coordinate (SCGC) formalism described earlier for computing the mass parameter for collective nuclear motion is cast into a form containing no explicit reference to the Hamiltonian. The expression is then specialized to the nuclear model of deformed harmonic oscillators. The usual Gaussian overlap approximation is eschewed in favor of direct evaluation of the appropriate matrix elements. Exchange terms are handled by a diagrammatic technique. The validity of certain assumptions made in the derivation of the mass formula is tested numerically. The effects of pairing and of short-range Jastrow correlations are investigated. The SCGC mass parameter is computed for several $N=Z$ nuclei and found to be smaller than either the cranking or the irrotational values, if no correlations are included. The inclusion of short-range correlations is shown to lead to important changes in the value of the mass parameter.

[NUCLEAR STRUCTURE Quadrupole mass parameter calculated. Self-cranked generator coordinate formalism. Correlations included. Compared to irrotational flow values.]

I. INTRODUCTION

In a previous paper,¹ hereafter referred to as I, we derived an expression for the mass parameter associated with collective nuclear quadrupole motion. A number of approximations and assumptions about the behavior of certain matrix elements was necessary, and it is the purpose of this paper to study in a simple model how well these matrix

elements conform to the expected behavior.

The idea of I was to modify the Hill-Wheeler projection technique² to incorporate the dynamics of the deforming system into the formalism. In particular the system is self-cranked in such a manner as to guarantee that the total energy is a minimum. Such a self-cranked generator coordinate (SCGC) approach yields two possible forms

for the mass parameter B ,

$$B_{\xi}^{-1}(\alpha) = - \frac{\int d\alpha' (\alpha | H - E | \alpha') (\alpha' - \alpha)^2}{\int d\alpha' (\alpha | \alpha')} - \frac{2 \left[\int d\alpha' (\alpha | (Q - \langle Q \rangle_{\alpha}) (H - E) | \alpha') (\alpha' - \alpha) \right]^2 / \int d\alpha' (\alpha | \alpha')}{\int d\alpha' (\alpha | (Q - \langle Q \rangle_{\alpha}) (H - E) (Q - \langle Q \rangle_{\alpha'}) | \alpha') d\alpha' + \int d\alpha' (\alpha | (Q - \langle Q \rangle_{\alpha})^2 (H - E) | \alpha')}, \quad (1)$$

where H is the total (microscopic) Hamiltonian of the nucleus, E the total energy, and $Q = \sum_{i=1}^A q_i$ the mass quadrupole moment operator. The rounded bras and kets refer to the intrinsic nuclear wave functions (Hartree-Fock, shell model, or exact) and $\alpha(\alpha')$ may be any convenient label denoting the deformation of the state. Below, the variable α is explicitly related to the potential deformation ϵ in a convenient way. The angular brackets require a coordinate space integration with respect to wave functions of the indicated

deformation. $B_{>}$ represents the form of the mass appropriate to the classical ($E > V$) region, and $B_{<}$ that appropriate to the classically forbidden ($E < V$) region.

The actual evaluation of Eq. (1) is complicated by the appearance of matrix elements having bras and kets corresponding to two different deformations. This means that the various exchange terms which would vanish in the case of an expectation value do not in general vanish here. It is still possible to study Eq. (1) numerically in

an approximate but simple way, and in Sec. II Eq. (1) is reduced to such a form suitable for calculation with, e.g., constrained Hartree-Bogolyubov wave functions. For the sake of simplicity and clarity the wave functions $|\alpha\rangle$ and $|\alpha'\rangle$ are assumed to be composed of deformed harmonic oscillators, but no spin-orbit coupling is included. The effects of pairing are included by way of the BCS formalism. Two-body correlations of the Jastrow type are also included. In Sec. III necessary formulas are compiled, in Sec. IV numerical results are given for particular matrix elements of interest, in Sec. V the SCGC mass of Eq. (1) is compared with the irrotational liquid drop model and the effects of correlation are shown; in Sec. VI a brief summary is given.

II. SIMPLIFIED MASS PARAMETER

Although deformed harmonic-oscillator wave functions are used ultimately, it is assumed for the moment that more realistic wave functions are available. Thus suppose that the intrinsic wave functions $|\alpha\rangle$ are very good to begin with (before projection), so that they nearly diagonalize $\mathcal{K} = H + \bar{\alpha}Q$. Here $\bar{\alpha}$ is a Lagrange multiplier chosen such that the solution has a specified quadrupole moment $\langle Q \rangle$, a function $\bar{\alpha}$. Then, at the extremum points in the potential energy curve characterized by $\bar{\alpha} = 0$,

$$(\alpha | (H - E) \approx 0 .$$

Commuting $(H - E)$ to the left everywhere it ap-

pears in Eq. (1) to act upon $(\alpha |$ yields

$$B_{>} = - \frac{i \int d\alpha' (\alpha | (Q - \langle Q \rangle) \dot{Q} | \alpha') + \int d\alpha' (\alpha | \dot{Q} | \alpha') (\alpha' - \alpha) \int d\alpha' (\alpha | \alpha')}{2 [\int d\alpha' (\alpha | \dot{Q} | \alpha') (\alpha' - \alpha)]^2} \quad (2a)$$

for $E > V$ and

$$B_{<} = \frac{i [2 \int d\alpha' (\alpha | \dot{Q} (Q - \langle Q \rangle) | \alpha') + \int d\alpha' (\alpha | (Q - \langle Q \rangle) \dot{Q} | \alpha') + \int d\alpha' (\alpha | \dot{Q} | \alpha') (\alpha' - \alpha) \int d\alpha' (\alpha | \alpha')]}{2 [\int d\alpha' (\alpha | \dot{Q} | \alpha') (\alpha' - \alpha)]^2} \quad (2b)$$

for $E < V$. Here

$$\dot{Q} = i[H, Q]. \quad (3)$$

Equation (2b) is included for the sake of completeness alone since for the harmonic oscillator the potential energy curve does not turn over with increasing α and consequently, only the energy region $E > V$ is appropriate. The Hamiltonian H is not explicit in either Eq. (2a) or (2b). In the following section the matrix elements in Eqs. (2) are specialized to the case of deformed harmonic-oscillator wave functions.

III. SOME NECESSARY FORMULAS

Equations (2) for the mass involve matrix elements of the operators

$$1, \quad (4a)$$

$$Q = \sum_{i=1}^A q_i, \quad (4b)$$

$$\dot{Q} = \sum_{i=1}^A \dot{q}_i = i[H, Q], \quad (4c)$$

$$Q\dot{Q} = \sum_{i,j=1}^A q_i \dot{q}_j, \quad (4d)$$

and

$$\dot{Q}Q = \sum_{i,j=1}^A \dot{q}_i q_j, \quad (4e)$$

each taken between states at different deformations. Consider the single-particle matrix elements. The simplest of these is just the overlap

$$\int \psi_{m,n,n_z}^*(\varphi\rho z; \alpha) \psi_{m',n',n'_z}(\varphi\rho z; \alpha') d\bar{r} \\ \equiv \langle mn n_z; \alpha | m' n' n'_z; \alpha' \rangle, \quad (5)$$

where α and α' label the deformation and in general $\alpha \neq \alpha'$. Since only cylindrically symmetric nuclear deformations are considered, the wave functions are given as functions of the cylindrical coordinates (φ, ρ, z) . Then n and n_z enumerate quanta in the ρ and z directions, respectively, and m is the z projection of angular momentum. Equation (5) may be factored as follows:

$$\langle mn n_z; \alpha | m' n' n'_z; \alpha' \rangle = \delta_{mm'} \langle R_n^m(\gamma\rho), R_{n'}^{m'}(\gamma'\rho) \rangle \\ \times \langle u_{n_z}(\lambda z), u_{n'_z}(\lambda' z) \rangle, \quad (6)$$

where $\gamma(\gamma')$ denotes the scale of the potential in the ρ direction and $\lambda(\lambda')$ that in the z direction. The requirement of conservation of nuclear volume

leads to the relation

$$\lambda\gamma^2 = \text{constant}. \quad (7)$$

The quantities, λ , γ are related to the frequencies ω_z and ω_ρ , in the z and ρ directions, respectively, by the equations

$$\lambda = \left(\frac{\mu\omega_z}{\hbar} \right)^{1/2}, \quad (8)$$

$$\gamma = \left(\frac{\mu\omega_\rho}{\hbar} \right)^{1/2},$$

where μ is the nucleon mass. Neutron and proton masses are taken to be equal to each other.

The wave functions in the z direction are one-dimensional harmonic oscillators

$$u_{n_z}(\lambda z) = \left(\frac{\lambda}{\pi^{1/2} 2^{n_z} n_z!} \right)^{1/2} e^{-\lambda^2 z^2/2} H_{n_z}(\lambda z), \quad (9)$$

where H_{n_z} is a Hermite polynomial. Using the generating function for Hermite polynomials,³ the

overlap is found to be

$$\int dz u_{n_z}(\lambda z) u_{n'_z}(\lambda' z) = \left(\frac{2\lambda\lambda'}{\lambda^2 + \lambda'^2} \right)^{1/2} \left(\frac{n_z! n'_z!}{2^{n_z + n'_z}} \right)^{1/2}$$

$$\times \sum_{\substack{k=0 \\ (n_z \leq n'_z)}}^{\leq n_z/2} \left(\frac{\lambda'^2 - \lambda^2}{\lambda'^2 + \lambda^2} \right)^{2k + (n'_z - n_z)/2} \left(\frac{4\lambda\lambda'}{\lambda'^2 + \lambda^2} \right)^{n_z - 2k} \frac{(-)^k}{k! [\frac{1}{2}(n'_z - n_z) + k]! [n_z - 2k]!}. \quad (10)$$

Equation (10) is valid if $n'_z - n_z$ is even (otherwise the overlap is zero), and if $n_z \leq n'_z$. If $n_z > n'_z$, the overlap may be found by exchanging n_z with n'_z and λ with λ' .

The wave functions in the ρ direction are the two-dimensional harmonic oscillators

$$R_n^m(\gamma\rho) = \gamma \left(\frac{2n!}{[(m+n)!]^3} \right)^{1/2} \exp(-\frac{1}{2}\gamma^2\rho^2) (\gamma\rho)^m L_n^m[(\gamma\rho)^2], \quad (11)$$

where L_n^m is a Laguerre polynomial. Using the generating function for the Laguerre polynomials,³ the overlap is found to be

$$\int d\rho R_n^m(\gamma\rho) R_{n'}^{m'}(\gamma'\rho) = \left(\frac{2\gamma\gamma'}{\gamma^2 + \gamma'^2} \right)^{m+1} \left(\frac{n! n'}{(m+n)! (m+n')!} \right)^{1/2}$$

$$\times \sum_{\substack{k=n \\ (n \geq n')}}^{n+n'} \frac{(m+k)!}{(n+n'-k)! (k-n)! (k-n')!} (-)^{n'-k} \left(\frac{\gamma^2 - \gamma'^2}{\gamma^2 + \gamma'^2} \right)^{2k - (n+n')}. \quad (12)$$

Equation (12) is valid if $n \geq n'$. If $n < n'$, the overlap may be found by interchanging n with n' and γ with γ' .

Consider now matrix elements of the quadrupole operator

$$q = 2z^2 - \rho^2, \quad (13)$$

namely

$$\langle mn_n | q | \overline{m'n'_n} \rangle = \delta_{mm'} [2 \langle mn | \overline{mn'} \rangle \langle n_z | z^2 | \overline{n'_z} \rangle - \langle n_z | \overline{n'_z} \rangle \langle mn | \rho^2 | \overline{mn'} \rangle], \quad (14)$$

where the bar indicates that the wave function depends upon either λ' or γ' . The overlap integrals in Eq. (14) have been computed above. Equation (14) may be rewritten as

$$\langle mn_n | q | \overline{m'n'_n} \rangle = \delta_{mm'} \left[2 \langle mn | \overline{mn'} \rangle \sum_{n''_z} \langle n_z | z^2 | n''_z \rangle \langle n''_z | \overline{n'_z} \rangle - \langle n_z | \overline{n'_z} \rangle \sum_{n''} \langle mn | \rho^2 | mn'' \rangle \langle mn'' | \overline{mn'} \rangle \right]. \quad (15)$$

Each sum will contain at most three terms. The nonvanishing matrix elements of ρ^2 are

$$\langle mn | \rho^2 | mn'' \rangle = \int d\rho R_n^m(\gamma\rho) \rho^2 R_{n''}^m(\gamma\rho)$$

$$= \begin{cases} -\frac{1}{\gamma^2} [(n+1)(m+n+1)]^{1/2}, & n'' = n+1 \\ \frac{1}{\gamma^2} (2n+m+1), & n'' = n \\ -\frac{1}{\gamma^2} [n(m+n)]^{1/2}, & n'' = n-1. \end{cases} \quad (16)$$

The nonvanishing matrix elements of z^2 are

$$\begin{aligned} \langle n_z | z^2 | n_z' \rangle &= \int dz u_{n_z}(\lambda z) z^2 u_{n_z'}(\lambda z) \\ &= \begin{cases} \frac{1}{\lambda^2} \frac{1}{2} [(n+2)(n+1)]^{1/2}, & n'' = n+2 \\ \frac{1}{\lambda^2} (n + \frac{1}{2}), & n'' = n \\ \frac{1}{\lambda^2} \frac{1}{2} [n(n-1)]^{1/2}, & n'' = n-2. \end{cases} \end{aligned} \quad (17)$$

The operator \dot{q} is taken to be the commutator of q with the kinetic energy part of the Hamiltonian $H = T + V$:

$$\dot{q} = i[T, q] = \frac{-2i}{\mu} \left[2z \frac{\partial}{\partial z} - \rho \frac{\partial}{\partial \rho} \right], \quad (18)$$

where μ is the nucleon mass. The matrix element of \dot{q} may be decomposed in a manner similar to Eq. (14). It is then necessary to know matrix elements of $z(\partial/\partial z)$ and $\rho(\partial/\partial \rho)$ between states belonging to the same Hamiltonian. The nonvanishing matrix elements of $\rho(\partial/\partial \rho)$ are:

$$\begin{aligned} \langle m n | \rho \frac{\partial}{\partial \rho} | m n'' \rangle &= \int d\rho \rho R_n^m(\gamma \rho) \rho \frac{\partial}{\partial \rho} R_n^{m''}(\gamma \rho) \\ &= \begin{cases} -[(n+1)(m+n+1)]^{1/2}, & n'' = n+1 \\ -1 & n'' = n \\ [n(m+n)]^{1/2}, & n'' = n-1 \end{cases} \end{aligned} \quad (19)$$

and the nonvanishing matrix elements of $z(\partial/\partial z)$ are:

$$\begin{aligned} \langle n_z | z \frac{\partial}{\partial z} | n_z' \rangle &= \int dz u_{n_z}(\lambda z) z \frac{\partial}{\partial z} u_{n_z'}(\lambda z) \\ &= \begin{cases} \frac{1}{2} [(n_z+1)(n_z+2)]^{1/2}, & n_z'' = n_z+2 \\ -\frac{1}{2}, & n_z'' = n_z \\ -\frac{1}{2} [n_z(n_z-1)]^{1/2}, & n_z'' = n_z-2. \end{cases} \end{aligned} \quad (20)$$

The generating functions of the Hermite and Laguerre polynomials were used in obtaining Eqs. (16), (17), (19), and (20).

The two particle operators of interest are $Q\dot{Q}$ and $\dot{Q}Q$. Their matrix elements are treated in a fashion similar to the above. Consider

$$Q\dot{Q} = \sum_{i,j=1}^A q_i \dot{q}_j. \quad (21)$$

If $i \neq j$, the matrix elements of (21) will reduce to products of the matrix elements of q and \dot{q} , which are discussed above. For the case $i = j$ the insertion of a complete set of states again reduces the problem to the evaluation of matrix elements already studied. The operator $\dot{Q}Q$ is handled in an entirely equivalent manner.

Attention may now be turned to the evaluation of matrix elements of the operators of Eqs. (4) with respect to the complete many-body nuclear wave functions. These wave functions are taken to be antisymmetrized combinations of single-particle functions. These latter functions are deformed harmonic oscillators. Furthermore, the effects of short-range residual interactions is simulated by means of the BCS pairing formalism. Jastrow-type correlations will be introduced at a later stage. Thus the basic wave function for an even-even nucleus may be written

$$\Psi(\vec{r}_1, \dots, \vec{r}_A) = \prod_{i=1}^{\infty} (u_i + v_i a_i^\dagger a_i^\dagger) |0\rangle, \quad (22)$$

where $u_i(v_i)$ is the probability amplitude that the

single-particle state i and time reversed state \bar{i} is unoccupied (occupied). The index i goes over neutrons and protons separately. The amplitudes u_i and v_i satisfy

$$u_i^2 + v_i^2 = 1. \quad (23)$$

The operator a_i^\dagger creates a wave function for the state i when it operates upon the particle vacuum. a_i annihilates such a state.

The BCS coefficients u_i, v_i , as well as the operators a_i^\dagger and a_i are functions of the deformation variable α' . Thus

$$\Psi(\bar{r}_1, \dots, \bar{r}_A) \equiv \Psi(\bar{r}_1, \dots, \bar{r}_A; \alpha') \equiv |\alpha'\rangle. \quad (24)$$

The occupation amplitudes were computed from a pairing strength G ranging from 0.3 to 0.5 MeV, the larger values for lighter nuclei. Since wave functions at all deformations are included in the definition of the mass B [Eq. (2)], deformation-dependent pairing strengths should in principle be employed. As little is known about the deformation dependence of G , the pairing strength is as-

sumed independent of the nuclear shape (see, however, Ref. 4). The number of proton or neutron states used in the pairing calculations was on the order of 12 states on each side of the Fermi level. The levels entering the calculation were chosen from the lowest members (at the desired deformation) of that group of states which included levels up through the two shells above the spherical Fermi level.

It is necessary to write down the many-body matrix elements of the operators, Eq. (4), in terms of the BCS coefficients u_i, v_i and the single-particle matrix elements discussed above. While it is not feasible, for a large- A system, to include all possible exchange terms, the many-body matrix elements can be expressed in an approximate fashion by considering all contributions through terms arising from each distinct pair of paired particles. Since neutrons and protons are considered separately, only neutrons are treated here. Protons are dealt with in a completely analogous way.

For the neutron overlap

$$\langle \alpha | \alpha' \rangle = \langle 0 | (u_1 + v_1 a_1 a_1^\dagger) (u_2 + v_2 a_2 a_2^\dagger) \cdots (u'_2 + v'_2 a'_2 a'_2^\dagger) (u'_1 + v'_1 a'_1 a'_1^\dagger) | 0 \rangle; \quad (25)$$

the lowest-order term is the direct term,

$$\prod_n (u_n u'_n + v_n v'_n \langle n | n \rangle^2),$$

where the primed quantities are functions of α' . Single-particle bras are understood to be functions of α , while single-particle kets are functions of α' . Use has been made of the anticommutation relation

$$\{a_i, a'_j^\dagger\} = \langle i | j \rangle. \quad (26)$$

The next terms to be considered arise from the contributions of each set of two pairs. In this case,

$$\langle \alpha | \alpha' \rangle = \prod_n (u_n u'_n + v_n v'_n \langle n | n \rangle^2) \times \left\{ 1 + \sum_{1 < 2} \frac{u_2 v_1 u'_1 v'_2 \langle 1 | 2 \rangle^2 + v_2 u_1 v'_1 u'_2 \langle 2 | 1 \rangle^2 + v_2 v_1 u'_2 v'_1 (\langle 2 | 1 \rangle^2 \langle 1 | 2 \rangle^2 - 2 \langle 2 | 2 \rangle \langle 1 | 1 \rangle \langle 2 | 1 \rangle \langle 1 | 2 \rangle)}{(u_2 u'_2 + v_2 v'_2 \langle 2 | 2 \rangle^2) (u_1 u'_1 + v_1 v'_1 \langle 1 | 1 \rangle^2)} \right\}. \quad (27)$$

Here the numerals 1, 2 are shorthand for n_1, n_2 . The overlap for the whole nucleus, including protons, is just the square of Eq. (27) if the number of neutrons equal the number of protons. This is the case considered here.

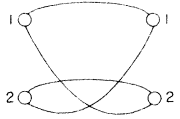
The various terms which enter Eq. (27) may be illustrated graphically in the following manner



$$\equiv v_1 v_2 v'_1 v'_2 \langle 2 | 2 \rangle^2 \langle 1 | 1 \rangle^2. \quad (28)$$

The numbers on the left of the diagram refer to orbitals of deformation α , while those on the right refer

to orbitals of deformation α' . The topmost horizontal line for each state represents the overlap matrix element for a $(j, +m_j)$ particle, the lower line that for the time reversed state $(j, -m_j)$. Here j, m_j are the angular momentum and z projection of the particle. The example above, for the two occupied pair states, gives the direct term. If the $(j_2, -m_{j_2})$ particle is exchanged with the $(j_1, -m_{j_1})$ particle, then



$$\equiv -v_1 v_2 v'_1 v'_2 \langle 2|2\rangle \langle 1|1\rangle \langle 1|2\rangle \langle 2|1\rangle. \quad (29)$$

If both particles are exchanged



$$\equiv +v_1 v_2 v'_1 v'_2 \langle 2|1\rangle^2 \langle 1|2\rangle^2. \quad (30)$$

The above examples all carry factors of $v_1 v_2 v'_1 v'_2$ since all states were occupied. However, another possible contribution would be



$$\equiv v_1 u_2 u'_1 v'_2 \langle 1|2\rangle^2. \quad (31)$$

The diagrammatic approach is unnecessary for the elucidation of the terms of the simple overlap $(\alpha|\alpha')$, but becomes useful in a systematic listing of the terms of $(\alpha|\Theta|\alpha')$, where Θ may be a two-, three-, or four-body operator.

The matrix elements of the single-particle operators Q and \dot{Q} may be written down in a manner very similar to that leading to Eq. (27). For the quadrupole operator Q

$$(\alpha|Q|\alpha') \approx 4(\alpha|\alpha') \left\{ \sum_{n_1} \frac{v_1 v'_1 q_{11} \langle 1|1\rangle}{d_1} + \sum_{n_1 \neq n_2} \frac{v_1 u_2 v'_2 v'_1 q_{12} \langle 1|2\rangle + v_1 v_2 v'_1 v'_2 (q_{12} \langle 1|2\rangle \langle 2|1\rangle^2 - q_{11} \langle 2|2\rangle \langle 1|2\rangle \langle 2|1\rangle - q_{12} \langle 1|1\rangle \langle 2|2\rangle \langle 2|1\rangle)}{d_1 d_2} \right\}, \quad (32)$$

where

$$q_{ij} \equiv \langle i|q|j\rangle$$

and

$$d_i = u_i u'_i + v_i v'_i \langle i|i\rangle^2.$$

In the result Eq. (32) we sum over one nuclear species only. An example of the type of diagram contained in Eq. (32) is



$$\equiv v_1 v_2 v'_1 v'_2 q_{21} \langle 2|1\rangle \langle 1|2\rangle^2, \quad (33)$$

where the line with the cross represents a matrix element of q .

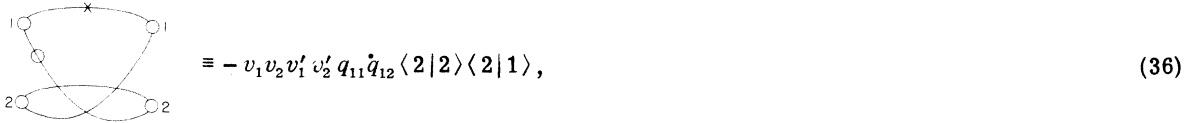
Finally to be considered are the quantities $(\alpha|Q\dot{Q}|\alpha')$ and $(\alpha|\dot{Q}Q|\alpha')$. The operator of the first expression is

$$Q\dot{Q} = \sum_{i,j} q_i \dot{q}_j = \sum_i q_i \dot{q}_i + \sum_{i \neq j} q_i \dot{q}_j. \quad (34)$$

The first sum on the right-hand side is a single-particle operator which has been treated above. It is useful to break up the second two-body term in such a way that neutron and proton coordinates are explicitly exhibited:

$$\sum_{i \neq j} q_i \dot{q}_j = \sum_{i_n \neq j_n} q_{i_n} \dot{q}_{j_n} + \sum_{i_p \neq j_p} q_{i_p} \dot{q}_{j_p} + \sum_{i_p, j_n} q_{i_p} \dot{q}_{j_n} + \sum_{i_n, j_p} q_{i_n} \dot{q}_{j_p} . \tag{35}$$

Matrix elements of the last two sums are products of the matrix elements discussed above. All contributions corresponding to the first two sums may be found from diagrams such as



where \times represents the matrix element of q and \circ and that of \dot{q} . The complete expression for $\langle \alpha | Q \dot{Q} | \alpha' \rangle$ is lengthy and is not reproduced here.

IV. OVERLAP MATRIX ELEMENTS

The derivation in I of Eq. (1) of this paper made use of certain assumptions about the shapes of overlap matrix elements $\langle \alpha | \Theta | \alpha' \rangle$, where Θ is a few particle operator. In particular it was assumed that $\langle \alpha | \Theta | \alpha' \rangle$ has a peaked shape about $\alpha' = \alpha$, in contrast to the diagonal matrix element $\langle \alpha' | \Theta | \alpha' \rangle$ which is supposed to be smoothly varying with α' . This is most clearly seen in the case of the normalization overlap $\langle \alpha | \alpha' \rangle$. If α' is slightly different from α , then the corresponding single-particle states i have overlaps ν_i with each other that are slightly less than unity. If an average overlap is ν , then $\langle \alpha | \alpha' \rangle$ is reduced from unity by a factor ν^A , where A is the number of nucleons.

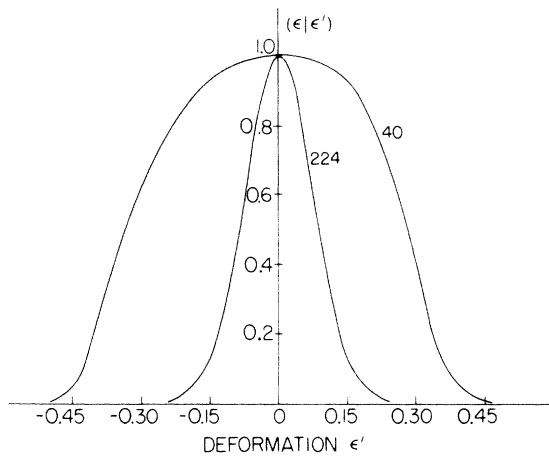


FIG. 1. The overlap of the many-body function $|\epsilon'\rangle = \Psi(\mathbf{r}_1, \dots, \mathbf{r}_A; \epsilon')$ with the wave function $|\epsilon\rangle$ is shown for two different mass numbers, $A = 40$ and $A = 224$. The quantity ϵ' is related to the potential deformation and is defined in the text. $\epsilon' = 0$ corresponds to zero potential deformation. $\epsilon = 0$.

If A is large, then ν^A may be quite small even though $\nu \approx 1$. This is a statement that $\langle \alpha | \alpha' \rangle$ is sharply peaked about $\alpha' = \alpha$. The approximation requiring the matrix element to be sharply peaked should then be better for heavier nuclei.

This argument of fast falloff as presented is strictly true only for small $|\alpha' - \alpha|$. When $\alpha' \neq \alpha$, in addition to the direct term

$$\langle \alpha | \alpha' \rangle = \prod_{i=1}^A \langle i; \alpha | i; \alpha' \rangle , \tag{37}$$

there are exchange terms present since in general $\langle i, \alpha | j, \alpha' \rangle \neq 0$. These terms appear as corrections to Eq. (37),

$$\langle \alpha | \alpha' \rangle = \prod_{i=1}^A \langle i; \alpha | i; \alpha' \rangle [1 + C_i(\alpha, \alpha')], \tag{38}$$

and their explicit form is given approximately in Eq. (27). For $\alpha' = \alpha$, $C_i = 0$. As $|\alpha' - \alpha|$ in-

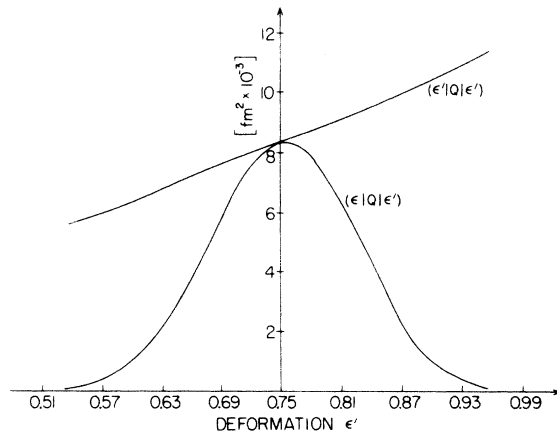


FIG. 2. The variation with deformation ϵ' of the matrix element $\langle \epsilon | Q | \epsilon' \rangle$ is compared with that of $\langle \epsilon' | Q | \epsilon \rangle$. $A = 224$.

creases, $|C_i|$ will increase. The direct term is dominant, however, and as shown below the exchange only modestly affects the falloff widths. These falloff patterns are well known in the cases of nuclear rotations⁵ and vibrations.⁶ In the latter case, however, the approach is usually to employ the "Gaussian overlap approximation" rather than to use the actual shape of the matrix element. The Gaussian assumption is discussed below.

The more complex overlap functions $(\alpha|\Theta|\alpha')$ are expected to behave in a manner similar to $(\alpha|\alpha')$ if Θ is a few particle operator. In that case the majority of the nucleons (the "core") enjoy the same overlap properties as in the normalization case, so that for large A the peaked property should obtain. There are cases where $(\alpha|\Theta|\alpha)$ will not be peaked, and in fact will vanish at $\alpha' = \alpha$; for example if Θ is an odd operator. The shape of the matrix element is then such that its absolute value rises from zero as $|\alpha' - \alpha|$ increases, but then decreases again quickly as the damping effect of the core nucleons comes into play.

Some of these results are shown in Figs. 1-7. Figure 1 shows the overlap matrix elements for a nucleus with equal numbers of protons and neutrons. Here the parameter α' is directly related to the potential deformation and is called ϵ' . The nucleon potential is taken to be⁷

$$V = \frac{1}{2} \mu [(x^2 + y^2) \omega_1^2 + z^2 \omega_z^2], \quad (39)$$

where

$$\omega_1 = \omega_0 (1 - \frac{1}{3} \epsilon)^{-1} \approx \omega_0 (1 + \frac{1}{3} \epsilon), \quad (40)$$

$$\omega_z = \omega_0 (1 - \frac{1}{3} \epsilon)^2 \approx \omega_0 (1 - \frac{2}{3} \epsilon),$$

and

$$\omega_1^2 \omega_z = \omega_0^3 = \text{constant}. \quad (41)$$

Positive ϵ decreases the frequency along the symmetry direction compared with the spherical case $\epsilon = 0$, so $\epsilon > 0$ refers to prolate distortions and $\epsilon < 0$ refers to oblate distortions. The curves in Fig. 1 are approximately symmetrical about $\epsilon' = 0$, and as expected the $A = 224$ width is narrower than that for $A = 40$. In fact, the curves oscillate slightly far out in the wings, but the amplitude is too small to be seen on the scale of the figure.

Figure 2 shows a comparison between the matrix elements $(\epsilon|Q|\epsilon')$ and $(\epsilon'|Q|\epsilon')$ for the $A = 224$ nucleus at $\epsilon = 0.75$. The diagonal matrix element is a smoothly varying function of ϵ' , while the overlap is peaked at $\epsilon' = \epsilon$. The curve corresponding to $(\epsilon'|Q|\epsilon')$ for the case of the unit operator $(\epsilon'|\epsilon')$ would be a horizontal line in Fig. 1.

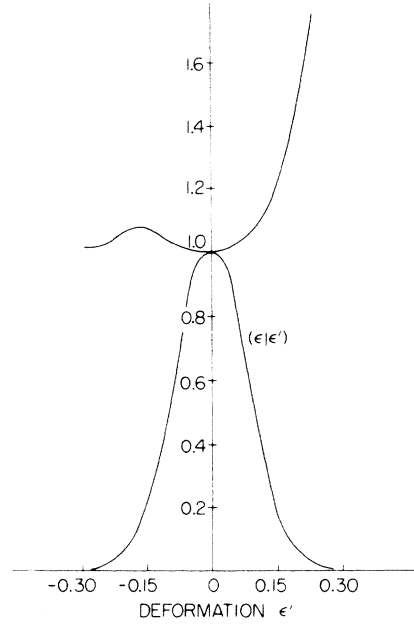


FIG. 3. The effect of particle exchange on the overlap is demonstrated. The lower curve shows the overlap with exchange contributions neglected. To obtain the overlap values with exchange, the lower curve must be multiplied by the upper curve. $A = 184$.

In Fig. 3 is shown the effect of particle exchange on the overlap $(\epsilon|\epsilon')$ at $\epsilon = 0$. The lower curve gives the falloff if no exchange is included. It is to be multiplied by the upper curve to get the proper shape for inclusion of exchange. At $\epsilon' = 0$ exchange has no effect because the single-particle orbitals i, j on opposite sides of the matrix element have vanishing overlap unless $i = j$. As $|\epsilon - \epsilon'|$ increases from zero, exchange

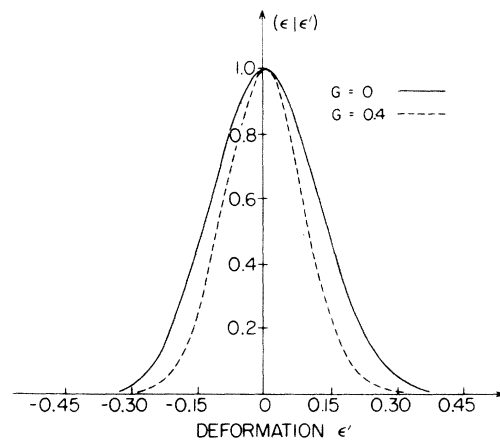


FIG. 4. The effect of pairing on the overlap is demonstrated. The solid curve is for the case of no pairing, while the dashed curve shows the effect of pairing, with strength $G = 0.4$ MeV. $A = 184$.

effects are felt. They tend to broaden the peak a bit. Although the exchange factor seems to be shooting up rapidly for prolate ($\epsilon' > 0$) deformation, the direct term is falling much more rapidly.

Pairing tends to have the opposite effect on the overlap; namely, it narrows the peak. In Fig. 4 this effect is shown for wave functions without pairing and for wave functions with a pairing strength of 0.4 MeV. Both functions are normalized to unity at $\epsilon' = 0$.

It was assumed in I that the width $\Delta(\alpha)$ of the normalization function $(\alpha|\alpha')$ was not rapidly varying with α . In Fig. 5 ($\epsilon|\epsilon'$) is plotted as a function of ϵ' for several values of ϵ corresponding to oblate, spherical, and prolate deformations. In Fig. 6 Δ is plotted as a function of ϵ' . The prolate and spherical widths ($\epsilon = 0.75, 0$) are not very different from each other. The oblate width ($\epsilon = -0.75$) is somewhat larger. The prolate deformations will generally be of the greatest interest.

In I it was suggested that the integrals over α' be carried out by an expansion technique which approximated the shape of $(\alpha|\Theta|\alpha')$, for small enough $|\alpha' - \alpha|$, by a Gaussian form

$$(\alpha|\Theta|\alpha') = e^{-(\alpha' - \alpha)^2 / \Delta^2} [A(\alpha) + B(\alpha; \alpha' - \alpha)], \quad (42)$$

where

$$B(\alpha, 0) = 0 \quad (43a)$$

and

$$A(\alpha) = (\alpha|\Theta|\alpha). \quad (43b)$$

Because of difficulties concerned with the con-

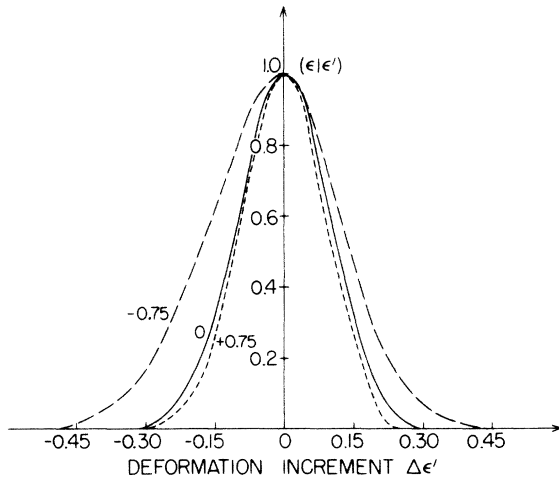


FIG. 5. The overlap $(\epsilon|\epsilon')$ is plotted as a function of ϵ' for several values of ϵ , corresponding to an oblate potential ($\epsilon = -0.75$), spherical potential ($\epsilon = 0$), and a prolate potential ($\epsilon = +0.75$). $A = 140$.

vergence of these types of expansions,⁶ and because of the difficulties of evaluating B , the functions $(\alpha|\Theta|\alpha')$ have been numerically integrated with respect to α' in the present paper according to the requirements of Eq. (1). Nevertheless, it is still of some interest to see how closely the overlap, for instance, may be approximated by a Gaussian form. In Fig. 7 the "exact" overlap $(\epsilon|\epsilon')$ for $A = 40$ is compared with both a Gaussian $\exp(-33/9 \epsilon'^2)$ and a modified Gaussian $\exp(-33/9 \epsilon'^2)(1 + 33/9 \epsilon'^3)$. The falloff distance comes from a consideration of the $A = 40$ configuration at spherical. These expressions are exact to order ϵ'^2 and ϵ'^3 , respectively. The modified, or skewed, Gaussian form is somewhat better than the pure Gaussian, but this approach is not pursued below.

As one check on the calculations, the overlap generated from Eq. (27), but with pairing turned off, is compared to an overlap expression computed without any initial reference to a pairing force, but including exchanges among all distinct groups of two, three, and four particles. The curve labeled "exact" in Fig. 7 was computed in the latter manner and agrees very well with the curve calculated from Eq. (27). The contribution from exchanges among all distinct groups of three and four particles was too small to significantly affect the curve of Fig. 7. This result supports the use of truncation as discussed in connection with Eq. (27).

V. MASS PARAMETER

In I the mass parameter B was identified in the Schrödinger equation for the wave function $f(\alpha)$ describing the quadrupole motion. The differential equation is approximately equivalent to an integral equation, derived from a variational principle. The approximation of going from the integral to the differential form involved the neglect of terms

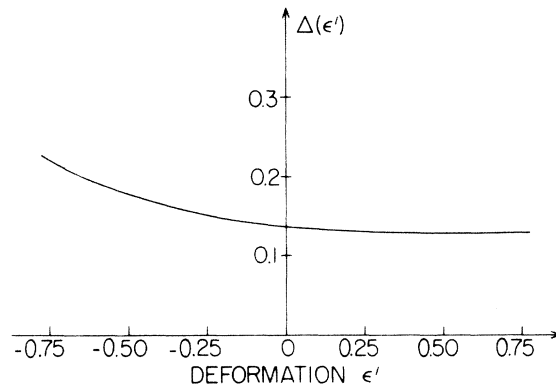


FIG. 6. The overlap width Δ is shown as a function of deformation ϵ' . $A = 140$.

containing derivatives of f higher than the second. The relevant parameter involved in the expansion of $f(\alpha')$ about $\alpha' = \alpha$ is Δ/L , where Δ is the falloff distance discussed above and $L = 2\pi/k$ is the local collective wavelength associated with f . Here

$$k \approx \left(\frac{2E_{\text{vib}} B}{\hbar^2} \right)^{1/2} \text{ fm}^{-2}. \quad (44)$$

E_{vib} is a typical vibrational energy and B is the effective mass. If Δ/L is small, then the neglect of higher derivatives of f is valid. To get an estimate of the size of this quantity, E_{vib} may be taken to be 1 MeV and B to be the irrotational result⁸

$$B^{(\text{irr})} \approx 0.036 \text{ MeV}/(\text{fm}^2 c^2). \quad (45)$$

This particular value is taken for the $A = 140$ system at spherical (see discussion of irrotational mass below). Converting the dimensionless falloff parameter Δ , as given in Fig. 6, to fm^2 :

$$\Delta/L \approx 0.06. \quad (46)$$

The true mass B may, in fact, be an order of magnitude larger than the irrotational estimate⁹ Eq. (45), in which case Δ/L is about three times

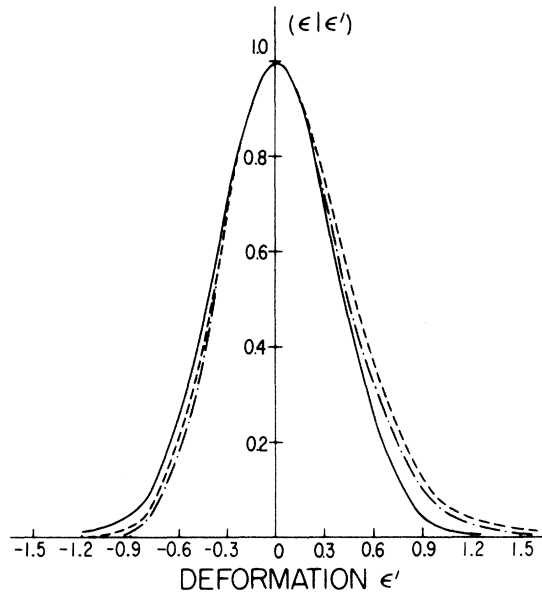


FIG. 7. The overlap for $A = 40$, with exchange, is compared to a Gaussian shape and to a skewed Gaussian. The solid line is the Gaussian shape, the dot-dashed line the skewed Gaussian, and the dashed line the exact overlap. The shape of the "exact" falloff curve differs from the $A = 40$ curve in Fig. 1 first, because pairing is not included in Fig. 7 and second, because of the number of single-particle states included. In the above figure the lowest ten states at spherical are used at all deformations, while in Fig. 1 the lowest ten states at each deformation are included.

larger than the result in Eq. (46), but still small.

The results for the mass parameter are shown in Fig. 8. The quantity actually plotted is B_0 , which corresponds to the inertia appropriate to the kinetic energy $(\frac{1}{2}) B_0 \dot{Q}^2$. The solid lines correspond to the irrotational flow result,⁸ while the dashed lines refer to the SCGC approach described in I and calculated according to a simplified prescription in this paper. Since the negative kinetic energy region at spherical [where Eqs. (2) are valid] is inaccessible in the present model, only values for B_0 are given.

The general trend of the curves with mass number A may be understood in terms of scaling effects. The irrotational result (at spherical) is⁸

$$B_0^{(\text{irr})} = \frac{\mu}{8A \langle r^2 \rangle}, \quad (47)$$

where μ is the nucleon mass. This quantity decreases with mass number in proportion to $A^{-5/3}$, so

$$B_0^{(\text{irr})} \sim A^{-5/3}. \quad (48)$$

The masses are plotted as a function of potential

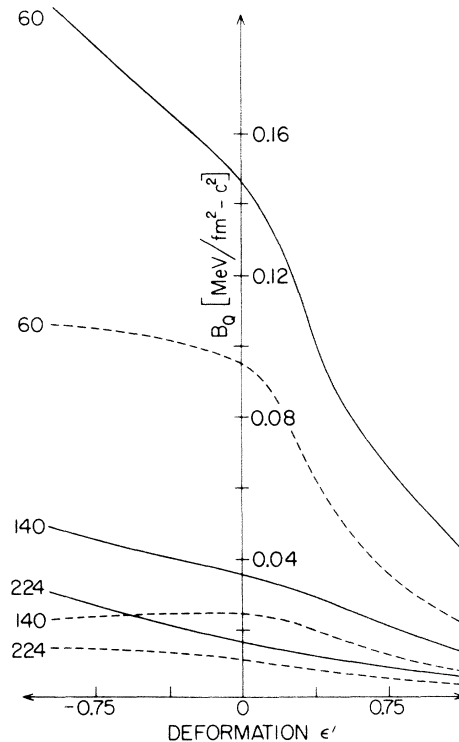


FIG. 8. The mass parameter for irrotational motion (solid line) is plotted vs the deformation parameter ϵ' and compared to the mass computed according to the self-creaked generator coordinate (SCGC) method (dashed line). The unpaired cranking model coincides at spherical with the irrotational result. The curves are labeled by mass number A .

deformation. However, the particular form (2) used for the projected mass is valid only at the equilibrium points in the potential energy curve. For the simple harmonic oscillator this means the projected result should be consulted only at $\epsilon' = 0$. The projected mass has been computed at a number of other deformations, with pairing included, to test the utility of the diagrammatic expansion of the matrix elements. The effect of increasing the pairing strength G from zero is to increase the mass by up to a factor of 2, but as G increases further the mass begins to decrease. Thus pairing appears to have less of an effect here than in the cranking model where an increase of B by an order of magnitude is indicated.⁹ Increasing by one shell the number of states from which levels are chosen for the pairing calculation increases $B_>$ by about 10%. Increasing the number of states actually used in the pairing calculation by 10 leads to a reduction in $B_>$ of about 10%. These figures are rough averages for various mass numbers and deformations.

The projected masses of Fig. 8 are to be compared with the irrotational flow value, which may be shown to be given by

$$B_Q^{(irr)} = \frac{\mu}{4[2A\langle r^2 \rangle + Q]} . \quad (49)$$

(See also Ref. 9.) Equation (47) is a special case of Eq. (49). One usually associates¹⁰ the values of Eq. (49) with a lower limit on the physically allowed values of the mass. The fact that the projected results turn out in the present case to be still lower suggests several conclusions.

The first of these is that the harmonic-oscillator model employed for the intrinsic wave function even with pairing may not contain sufficient correlations to provide for the possibility of the type of collective motion considered here. The diagonality assumption on the Hamiltonian, leading to Eqs. (2), neglects those features of H which would tend to produce a more correlated wave function. (Note that below we study the effects of Jastrow-type correlations.) Looked at in another way, the approximation $(H - E)|\alpha\rangle \approx 0$, for very simple wave functions $|\alpha\rangle$, implies that the solution to the wave equation is known so well *a priori* that no room is left for the model to contain the possibility of collective motion. It would be desirable to recompute the mass with more realistic wave functions, retaining explicit reference to the many-body Hamiltonian H , as in Eq. (1).

One improvement on the diagonality assumption would be to account explicitly for the extra vibrational kinetic part ΔE of the total energy, which is otherwise neglected (neglect of kinetic effects

on the kinetic parameter itself). In this case

$$(H - E_0)|\alpha\rangle \approx -\Delta E|\alpha\rangle . \quad (50)$$

At equilibrium it may be shown that

$$B_>(\Delta E) = B_>(0) + \Delta E t , \quad (51)$$

where t is positive. Thus kinetic effects do appear to increase $B_>$, but at least for the $A = 40$ case, where t was computed, $\Delta E t$ is only a few percent of $B_>(0)$.

Finally, there is the question of why the SCGC result should disagree with that of the cranking approach. For a spherical harmonic oscillator (no pairing) the cranking result¹¹ is the same⁸ as that given by the irrotational liquid drop model. The addition of pairing increases the cranking result. The present projected mass is thus less than the cranking prediction. In the cranking approach the speed of cranking is controlled externally. If the system is cranked slowly enough, then the computed mass is expected to be correct in the sense that it is a perturbation theoretic result and the perturbation is small. The formalism for the SCGC mass, however, does not work this way. The system is self-cranked in such a way as to minimize the energy. The collective velocity is nowhere explicit, and is not necessarily equivalent to the cranking velocity.

Furthermore, the derivation of the vibrational cranking result (time-dependent perturbation theory) suffers from difficulties attendant upon a time integration of the Schrödinger equation. In particular under the usual approximation the time variation of the shape variables $\alpha(t)$, and consequently the nonperiodic variation of the wave functions and energies, is neglected. These approximations are circumvented in the projection approach as described in I. It will be useful to see by way of numerical integration¹² how valid such approximations are for the cranking model.

The effects of correlations of the Jastrow type may be introduced in a relatively simple manner. Such correlations can be expected to affect the falloff distance Δ . From an examination of Eq. (2a) it is evident that the denominator depends upon Δ according to Δ^4 , while terms in the numerator are proportional to Δ^0 and Δ^2 . Thus an increase in the sharpness of the falloff curve should lead to a larger value of $B_>$. With this in mind, the dependence of Δ upon the presence of correlations has been studied. Note from this argument that Fig. 4 indicates directly that at least for a moderate value of the pairing strength, the mass parameter should increase above the unpaired value. This is the observed behavior.

The pair correlation function is taken to be of

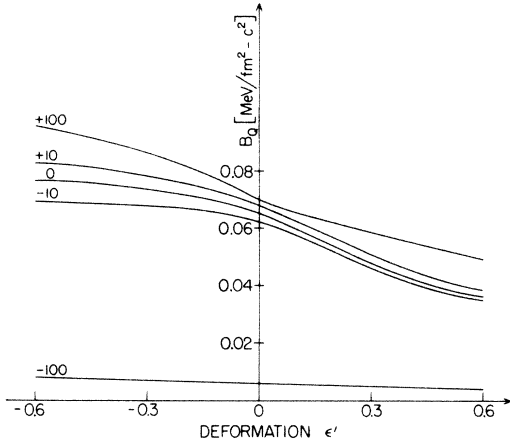


FIG. 9. The mass parameter calculated according to the SCGC method, with short-range correlations included, is plotted for several different values of the product ζd . Positive values of ζd correspond to an attractive short-range interaction. The uncorrelated values ($\zeta d = 0$) differ somewhat from the values for $A = 60$ of Fig. 8 due to a difference in pairing strength used. In this figure $G = 0.5$ MeV.

the δ -function form, thus

$$\psi_{ab}(\vec{r}_1, \vec{r}_2) \equiv \phi_a(\vec{r}_1) \phi_b(\vec{r}_2) [1 - \zeta \delta(\vec{r}_1 - \vec{r}_2)], \quad (52)$$

where $\phi_a(\vec{r}_1) \equiv \phi_a(\vec{r}_1; \alpha) \equiv |\alpha\rangle$ is a single-particle state and ζ gives the strength of the correlation. The normalized (pair) overlap is then

$$\langle \psi_{ab}(\alpha) | \psi_{ab}(\alpha') \rangle = \langle a | a \rangle \langle b | b \rangle [1 - \zeta g_{ab}(\alpha, \alpha')], \quad (53)$$

where the convention is that bras are functions of α and kets functions of α' , and

$$g_{ab} \equiv \int d\vec{r} [2h_{ab}(\vec{r}; \alpha, \alpha') - h_{ab}(\vec{r}; \alpha, \alpha) - h_{ab}(\vec{r}; \alpha', \alpha')]. \quad (54)$$

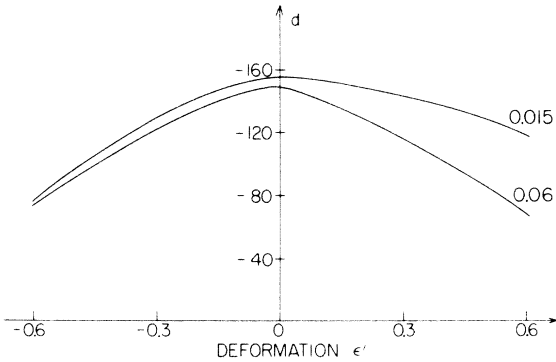


FIG. 10. The correlation factor d is plotted against deformation for two choices of the increment $\delta\epsilon$ [see Eq. (57)]. This graph may be used in conjunction with the value of ζ to find the value of the mass parameter in Fig. 9.

Finally

$$h_{ab}(\vec{r}; \alpha, \alpha') \equiv \frac{\phi_a^*(\alpha) \phi_b^*(\alpha) \phi_a(\alpha') \phi_b(\alpha')}{\langle a | a \rangle \langle b | b \rangle}. \quad (55)$$

Equation (54) must be summed over all pairs to give

$$g(\alpha, \alpha') = 12 \sum_{a \leq b} g_{ab}(\alpha, \alpha'). \quad (56)$$

The many particle overlap is then modified by a factor of the approximate form

$$1 - \zeta d(\alpha' - \alpha)^2 \approx \exp[-\zeta d(\alpha' - \alpha)^2] \quad (57)$$

to emphasize that corrections to the overlap only are under consideration. Here d is given by

$$d = \frac{g(\alpha, \alpha + \delta\alpha) + g(\alpha, \alpha - \delta\alpha)}{2(\delta\alpha)^2} \quad (58)$$

and

$$\delta\alpha = \alpha' - \alpha. \quad (59)$$

In Fig. 9 the mass parameter for $A = 60$ is plotted against the deformation variable $\alpha' \equiv \epsilon'$ for several values of the product ζd . Positive ζd leads to a decrease in the overlap width, and consequently, to an increase in the mass. A negative value for ζd has the opposite effect. The indication is that the flow characteristics are quite dependent upon the type of two-body correlation.

In Fig. 10 the quantity d of Eq. (58) is plotted against deformation. The goodness of the Gaussian approximation is indicated by the dependence of d upon the chosen value of the increment $\delta\epsilon$. The function d is shown for two choices of $\delta\epsilon$.

For any given value of ζ , the corresponding mass parameter may be interpolated on Fig. 9. Thus a positive value of $\zeta = 1 \text{ fm}^3$, which corresponds to a repulsive particle force at short distances, leads to a negative product at spherical $\zeta d \approx -155$ and consequently to a lowering of the mass parameter from the uncorrelated value. Conversely, choosing ζ to be negative, corresponding to an attractive force, raises the mass parameter.

These results emphasize the importance when calculating the mass parameter of using wave functions which contain realistic information about the contribution of the short-range forces to the flow pattern. The pure harmonic-oscillator wave functions employed in the bulk of this work are deficient in this respect. A large step in the right direction would be to use Hartree-Fock wave functions and retain explicit reference to the microscopic Hamiltonian H .

VI. SUMMARY

The behavior of certain matrix elements which enter into the theory of the mass parameter for collective quadrupole motion (see I) have been studied using deformed harmonic-oscillator wave

functions. These matrix elements include $(\epsilon|\epsilon')$, as well as those of the form $(\epsilon'|\Theta|\epsilon')$ and $(\epsilon|\Theta|\epsilon')$, where Θ is a few-body operator. The actual evaluation of the nondiagonal matrix element $(\epsilon|\Theta|\epsilon')$ is complicated by the existence of the many exchange terms which ordinarily vanish for $\epsilon = \epsilon'$. Introduction of pairing further complicates the picture. Both exchange and pairing contributions, however, may be organized in a straightforward way by the use of a diagrammatic technique. The calculations were carried out and the expected falloff behavior of these quantities as functions of ϵ' was verified. The nondiagonal matrices are peaked at $\epsilon' = \epsilon$ and vary more quickly with ϵ' than the diagonal matrices $(\epsilon'|\Theta|\epsilon')$. The sharpness of the falloff becomes more pronounced as the mass number A increases. Pairing and exchange tend to narrow and broaden the curves, respectively, but do not alter the general features.

The falloff distance, Δ , was found not to have a strong dependence on deformation, especially for spherical prolate deformations. This feature had been already incorporated in the development of the formalism in I.

The requirement that the derivatives of the collective wave function f higher than the second be neglected is related to the smallness of the quantity Δ/L , where L denotes the local collective wavelength. This quantity can be expected to be less than about 0.2 on the basis of estimates above.

Finally, the mass parameter itself was computed. The general expression for B_{\geq} was reduced to a simplified form which contained no explicit reference to the many-body Hamiltonian H . The accompanying approximations restrict the range of validity of the results in the present case to the spherical point $\epsilon = 0$. The mass, nevertheless, has been computed at a number of different deformations to show the utility of working with the truncated exchange expansion as derived from the

diagrammatic approach. Only the expression B_{\geq} has been given since the region $E < V$ at spherical is inaccessible in the harmonic-oscillator model.

The mass B_{\geq} was compared with the irrotational flow result $B^{(irr)}$ for several A values and was shown to be smaller. The cranking result at spherical for a system of harmonic oscillators reproduces the irrotational mass so B_{\geq} is less than either $B^{(irr)}$ or $B^{(crank)}$. Since $B^{(irr)}$ is usually considered to be a lower limit for physically allowed inertia, there is the question of why $B_{\geq} < B^{(irr)}$. Rough estimates indicate that this is probably not due to neglected kinetic effects on B_{\geq} , but may be related to the use of exact relations between the Hamiltonian H and the state $|\alpha\rangle$ or to the simplicity of the harmonic-oscillator basis. To study this last point, Jastrow-type correlations were introduced and found to give important modifications to B_{\geq} .

The SCGC approach is in some ways related to the cranking approach, but the system is cranked self-consistently in a way which yields the best energy. Thus, the cranking mechanisms of the two methods differ, with the SCGC result being derived in a quantum mechanical way. Assumptions about the time dependence of the deformation parameters which are necessary for the usual derivation of the cranking results are circumvented in the present approach. Consequently, the results in Fig. 8 may cast some suspicion on the validity of the cranking model.

With the basic assumptions of I borne out by the present calculations, it would be interesting to redo the calculations of the mass (including $B_{<}$) with more realistic wave functions.

We would like to acknowledge interesting and helpful discussions with Professor Sir Rudolf Peierls, Professor Ulrich Mosel, and Professor Gottfried Holzwarth.

*Work supported in part by the National Science Foundation Grant No. GP-28027 and the U.S. Atomic Energy Commission.

¹P. K. Haff and L. Wilets, Phys. Rev. C **7**, 951 (1973).

²D. L. Hill and J. A. Wheeler, Phys. Rev. **89**, 1106 (1953); J. J. Griffin and J. A. Wheeler, *ibid.*, **108**, 311 (1957); R. E. Peierls and J. Yoccoz, Proc. Phys. Soc. **70**, 381 (1957).

³P. M. Morse and H. Feshbach, *Methods of Theoretical Physics* (McGraw-Hill, New York, 1953), Part I.

⁴R. C. Kennedy, L. Wilets, and E. M. Henley, Phys. Rev. Lett. **12**, 36 (1964).

⁵Y. Y. Sharon, Ph.D. thesis, Princeton University, 1965 (unpublished).

⁶A. Klein, in *Dynamic Structure of Nuclear States*, edited by D. J. Rowe *et al.* (Univ. of Toronto Press, Canada, 1971).

⁷S. G. Nilsson, C. F. Tsang, A. Sobiczewski, Z. Szymanski, S. Wycech, C. Gustafson, I.-L. Lamm, P. Möller, and B. Nilsson, Nucl. Phys. **A131**, 1 (1969).

⁸L. Wilets, *Theories of Nuclear Fission* (Clarendon, Oxford, 1964); D. J. Rowe, *Nuclear Collective Motion* (Metheun, London, 1970).

⁹A. Sobiczewski, Z. Szymanski, S. Wycech, S. G. Nilsson, J. R. Nix, C. F. Tsang, C. Gustafson, P. Möller, and B. Nilsson, Nucl. Phys. **A131**, 67 (1969).

¹⁰J. R. Nix, Annu. Rev. Nucl. Sci. **22**, 65 (1972).

¹¹D. R. Inglis, Phys. Rev. **96**, 1059 (1954); **97**, 701 (1955).

¹²G. Schütte and L. Wilets, in Third International Atomic Energy Agency Symposium on Physics and Chemistry of Fission, Rochester, 1973 (to be published); and in preparation.